SCIENCE CHINA
Physics, Mechanics & Astronomy

• Review •
Progress of Projects Supported by NSFC · Spintronics

January 2013 Vol.56 No.1: 99–110
doi: 10.1007/s11433-012-4959-3

Enhancement of the Curie temperature of ferromagnetic semiconductor (Ga,Mn)As

WANG HaiLong, CHEN Lin & ZHAO JianHua*

State Key Laboratory of Superlattices and Microstructures, Institute of Semiconductors, Chinese Academy of Sciences, Beijing 100083, China

Received October 15, 2012; accepted November 23, 2012; published online December 26, 2012

In this review article, we review the progress made in the past several years mainly regarding the efforts devoted to increasing the Curie temperature (T_C) of (Ga,Mn)As, which is most widely considered as the prototype ferromagnetic semiconductor. Heavy Mn doping, nanostructure engineering and post-growth annealing which increase T_C are described in detail.

magnetic semiconductors, magnetic properties of nanostructures, magnetotransport phenomena, molecular-beam epitaxy

PACS number(s): 75.50.Pp, 75.75.+a, 75.47.-m, 81.15.Hi

Citation: Wang H L, Chen L, Zhao J H. Enhancement of the Curie temperature of ferromagnetic semiconductor (Ga,Mn)As. Sci China-Phys Mech Astron, 2013, 56: 99–110, doi: 10.1007/s11433-012-4959-3

1 Introduction

Semiconductors and magnetic materials are two of the most important branches of condensed matter physics, which have major roles in the modern information technology [1]. Utilizing the sensitivity of semiconductor properties to many kinds of defects like impurity atoms and the diversities of material structures like p-n junctions, information processing has been highly developed. On the other hand, due to the nonvolatility of magnetism, magnetic materials are extensively used for information storage. However, the rapid development achieved by exponentially increasing the density of relevant devices per unit area is approaching its limitation [2]. Meanwhile, the needs for high processing speed, high integration density, low power consumption and multifunctionalities are becoming more urgent [2]. The progress achieved by miniaturization of electronic devices cannot continue forever. Therefore, the solutions should consider the possibility to exploit the new carrier of information beside the charges. One of the most promising ways to meet the requirements is integrating ferromagnetism into semiconductors, using both the charges and spins in one material system which yields the field of ferromagnetic semiconductors [3].

Looking upon the history back to the 1960s, the ferromagnetic semiconductors can be roughly divided into three stages [4]. The first one is also known as the concentrated magnetic semiconductors since the magnetic atoms reside on every corresponding lattice site. EuO and EuS with rock-salt structure are the two representatives. They have large magnetic moments and strongly depend on the external magnetic field around the metal-insulator transition point. Through doping, they can also vary the carrier concentration to match the conductance of conventional semiconductors [5]. However, the relatively low Curie temperatures (T_C) and difficulties to grow high quality material structures restrict its application [4]. Researchers began to concern the magnetically doped II-VI semiconductors such as (Zn,Mn)Se and (Cd,Mn)Te in the late 1970s [6]. The II-VI semiconductors can be easily doped with Mn, introducing local spins. Thus, many spin related phenomena can

*Corresponding author (email: jhzhao@red.semi.ac.cn)

be tested on the basis of standard semiconductors. Unfortunately, the interactions between the localized magnetic moments are dominantly antiferromagnetic. It is also difficult to dope these materials into p-type or n-type, which makes it not so attractive. Since the late 1980s, using the low-temperature molecular-beam epitaxy (LT-MBE) technique, III-V ferromagnetic semiconductors such as (In,Mn)As and (Ga,Mn)As with the composition of magnetic atoms far beyond the thermal-equilibrium solubility limits were successfully prepared [7–9]. The substitutional divalent Mn atoms maintaining the lattice structure of the host semiconductors provide both holes and local moments [10,11]. More interestingly, theoretical and experimental evidences show that the ferromagnetism is mediated by delocalized holes residing in the valence band [12,13]. Recent results have been reported on these material systems, but whether T_C can be raised above the room temperature is a key issue [1].

(Ga,Mn)As has been the most deeply studied ferromagnetic semiconductor since it was first prepared in 1996 [9]. A series of outstanding functionalities have been demonstrated at low temperature, such as spin injection into nonmagnetic semiconductors [14], tunneling magnetoresistance [15], electric field and electric current manipulation of magnetism [13,16–19], and current induced domain displacement [20]. Moreover, great effort has been devoted to the enhancement of T_C of (Ga,Mn)As [21–26]. A series of experiments have been presented since the initial 60 K of T_C reported by Ohno et al. [9] in 1996: as-grown (Ga,Mn)As with T_C limited to 110 K because of the hole concentration compensated by defects was also reported by Ohno [3] in 1998, and by post-growth annealing, T_C ~ 160 K in (Ga,Mn)As/GaAs/(Ga,Mn)As trilayer [24] and T_C ~ 173 K were achieved by Ohno, Gallagher and Tanaka and others, respectively. It gradually reached ~ 185 K. However, the record reported up to now is 191 K in (Ga,Mn)As films [27] and 200 K in (Ga,Mn)As patterned nanowires [28], still far below room temperature. Figure 1 shows the timeline of the breakthroughs of T_C of (Ga,Mn) As, from which we can see that T_C increases very slowly in recent years.

In this review article, we review the typical methods implemented for the enhancement of T_C of (Ga,Mn)As within two theoretical scenarios, emphasizing on the heavy Mn doping [27] and nanostructure engineering which improve the efficiency of post-growth annealing [28].

2 Methods for enhancing T_C of (Ga,Mn)As

There are two major band pictures for the (Ga,Mn)As, both of which explain plenty of observations [29]. The fundamental difference focuses on whether the holes mediating the ferromagnetic interaction reside in an impurity band or a weakly disordered valence band [30]. The former one

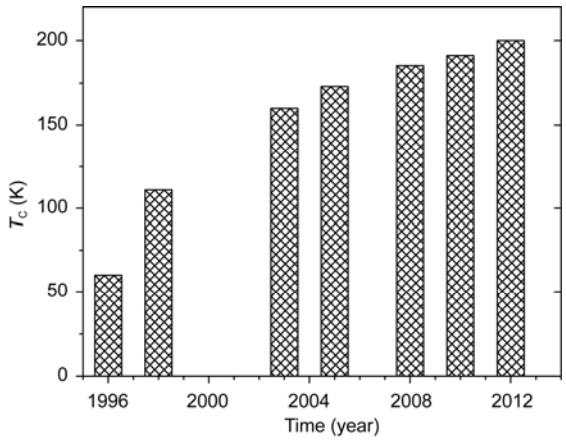

Figure 1 Timeline of the progress in the enhancement of T_C of ferromagnetic semiconductor (Ga,Mn)As.

assumes that the holes exist in a Mn-derived impurity band even for high Mn concentrations, while the latter states that the separated impurity band does not exist for Mn concentration higher than ~ 1%–2%. Both of them support the hole-mediated ferromagnetism scheme, providing the theoretical explanations for the electric-field manipulation of T_C.

In the impurity band regime, the location of the Fermi level determines the level of localization of the impurity band holes, thus determining T_C. The key point is tuning the Fermi level to the middle of the impurity band, where the hole states are the most extended [30]. Several specific methods to tune the location of Fermi level are proposed, such as appropriate control of the concentration of Mn interstitials (Mn_I), co-doping with donor ions like carbon and silicon to reduce the self-compensating Mn_I [31–33], or modulation doping. Besides, changing the binding energy of Mn acceptors can alter the location and width of the impurity band, thereby improving the mobility of the impurity band holes, resulting in the enhancement of T_C.

In the valence band regime, based on the *p-d* Zener model within the mean-field approximation [12,34], T_C of (Ga,Mn)As is proportional to the x_{eff} and $p^{1/3}$, where x_{eff} and p represent the effective concentration of Mn and the hole concentration, respectively. The expanded theory predicts that T_C depends on x_{eff} and p monotonically [35]. These theories predict that room temperature T_C is possible when x_{eff} and p are large enough, for example, when x_{eff} =12.5% and $p = 3.5\times10^{20}$ cm^{-3} [12,34]. However, some unwanted impurities also form during the LT-MBE growth of (Ga,Mn)As, such as arsenic antisites (As_{Ga}) and Mn_I shown in Figure 2 [36]. Both the As_{Ga} and Mn_I defects act as positively charged double-donors compensating the holes generated by the substitutional Mn (Mn_{Ga}). Morever, the Mn_I cation will couple with the adjacent Mn_{Ga} anion, making an antiferromagnetic superexchange contribution to the near-neighbor Mn_{Ga}-Mn_{Ga} ferromagnetic interaction [1,35]. Thus it can readily be seen that the direct methods to raise T_C are increasing the x_{eff} and p which involves optimizing the

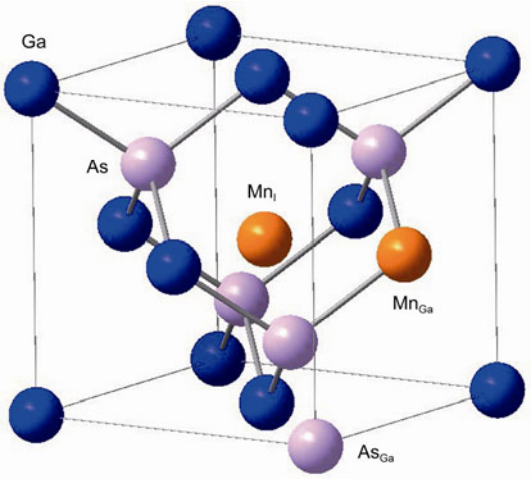

Figure 2 Unit cell of (Ga,Mn)As showing the lattice structure and defects like substitutional Mn, interstitial Mn and arsenic antisites.

growth conditions for heavy Mn doping, eliminating As_{Ga} and Mn_I and increasing hole concentration by co-doping.

Co-doping with various elements such Be, C and Cr was studied extensively in the hope of increasing the hole concentration by adding acceptors directly. Disappointingly, there is not breakthrough using this method. Complex defects were formed during the Be co-doping, which made the hole concentration even lower than doping Mn solely, and then lower T_C [37,38]. Park et al. [39] reported 280 K of T_C by implanting Mn into p^+-GaAs:C samples, but the metal-insulator transition phenomenon was not observed in these samples. Also there was not convincing evidence that the high temperature ferromagnetism was contributed by (Ga,Mn)As. As for the co-doping with another transition metal like Cr, the samples change from metallic side to insulating side with higher Cr content, and T_C decreases [40].

Many methods to realize higher Mn doping are proposed like using high-index substrates [41,42] and lowering the growth temperature further more [27]. The problem in these regimes is that a large fraction of Mn is the Mn_I, which makes T_C remain at 110 K for several years [1,3]. Then T_C went up to a higher level because of the discovery that post-growth annealing at the temperature roughly around or slightly below the growth temperature makes the Mn_I diffuse out in the atmosphere of air or O_2 efficiently and thus raise the T_C to 173 K [43,44]. It is worth noting that the As_{Ga} defects remain stable state up to about 450°C [45], at which post-growth annealing ruins the (Ga,Mn)As sample with the formation of other phases like hexagonal MnAs. Therefore, the stoichiometry of the deposited layer should be carefully controlled during LT-MBE growth. After T_C reached 185 K [46], no improvement had been reported until it was recently observed that 191 K of T_C in annealed (Ga,Mn)As thin films can be achieved under precisely controlled growth conditions using heavy Mn doping [27].

It is known that the annealing procedure under relatively low annealing temperature resulting in the passivation of the out-diffused Mn_I at the epilayer surface [21–25], exists a saturation point at which further annealing does not improve T_C, as shown in Figure 3. When annealed at higher temperature, T_C will usually decrease possibly because of the clustering of Mn_{Ga} atoms [47–50]. Based on this reality, (Ga,Mn)As nanowires which have larger percentage of free surface were prepared based on heavy Mn doping thin films using electron-beam lithography (EBL) technique. T_C as high as 200 K was obtained in the 300 nm wide patterned nanowire [28].

Moreover, Nazmul et al. [51] observed 250 K of T_C in the heterostructures consisting of Mn delta doped GaAs, but the Mn distribution is totally different from the one we discussed above.

Recently, T_C in a 5 nm (Ga,Mn)As thin film enhanced by nearly 100% because of the magnetic proximity effect was presented [52]. It considers the magnetic improvement of the ferromagnetic interaction by the adjacent ferromagnetic metal layer, which requires smooth and abrupt metal-semiconductor interface, involving very low temperature growth, typically room temperature, thus high T_C of as-grown samples are one of the most difficult issues. It may provide a good method to obtain high T_C in the future spintronic devices, but similar results have not been reported in high T_C samples yet.

In the following sections, the heavy Mn doping and nanostructure engineering will be described in details.

3 Heavy Mn doping

As discussed above, in order to dope Mn as much as possible and keep harmful defects at minimum, careful tuning of the growth conditions such as smooth buffer layer, substrate temperature, and V/III beam equivalent (BEP) ratio should be done during the LT-MBE growth. Several groups have shown that heavy Mn doping with the nominal Mn concentration between 15% and 20% is possible [44,53–56]. In order to avoid the formation of the second phase, the thickness of the heavily Mn-doped film is usually less than 100 nm and the growth temperature is among 150–200°C.

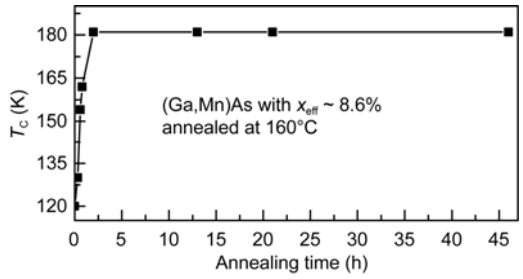

Figure 3 Annealing time dependence of T_C of (Ga,Mn)As film with x_{eff} ~ 8.6%, the annealing temperature is 160°C [28].

Note that the growth conditions would be MBE system dependent, but once they are built-up, the results are reproducible. For instance, Mack et al. [55] reported that heavily alloyed, 100 nm $Ga_{1-x}Mn_xAs$ ($0.1<x<0.22$) with highest T_C ~ 165 K can be obtained reproducibly by a combinatorial technique to achieve stoichiometry. Moreover, Chiba et al. [53] also showed that the nominal concentration x_{nomi} of Mn in (Ga,Mn)As can reach up to 20% by reducing substrate temperature to 170°C and thickness to 5 nm. However, the T_C of 20% Mn-doped sample is only 118 K determined by magnetotransport measurements, much lower than the theoretically predicted 345 K with the parameter $x_{eff} = 0.091 \pm 0.006$ and $p \sim 8\times10^{20}$ cm^{-3}. In their analysis, the As_{Ga} defects were not considered, which could be an important factor because of the high V/III BEP ratio (between 25 and 30) and low growth temperature they used during the growth.

To increase T_C of (Ga,Mn)As, our group has also done a series of work on the MBE preparation of heavily Mn-doped (Ga,Mn)As films, and successfully obtained the single phase (Ga,Mn)As films with the thickness from 5 to 75 nm. The typical high-resolution cross-sectional transmission electron microscopy (HRTEM) image (Figure 4(a)) of an 15 nm $Ga_{1-x}Mn_xAs$ film with x = 25% indicate a sharp interface between (Ga,Mn)As and GaAs and a high-quality (Ga,Mn)As single crystalline layer. No any MnAs clusters in the (Ga,Mn)As matrix can be seen. Both high-resolution X-ray reflection spectra (Figure 4(b)) and high-resolution X-ray diffraction (HRXRD) spectrum (the inset of Figure 4 (b)) of 15 nm heavy Mn doping $Ga_{1-x}Mn_xAs$ films also reveal their high quality and homogeneity.

In order to exclude the presence of secondary phases which can easily precipitate at such high Mn doping levels, we have characterized these films by ferromagnetic resonance (FMR) spectroscopy [57]. This spectroscopy allows a detection of ferromagnetic precipitates even of nanometer size, which can easily escape detection by X-ray analysis. As shown in Figure 5, we can see a typical X-band spectrum of a 15 nm $Ga_{1-x}Mn_xAs$ film with x_{nomi} = 25%. We observe only the uniform mode single line spectrum of the ferromagnetic (Ga,Mn)As phase with a large field scan from 0 to 18 kOe and no evidence for the presence of any ferromagnetic precipitate such as MnAs. The inset of Figure 5 is the angular variation in the FMR resonance field for an out-of-plane variation (squares), and a theoretical fit (line). The X-band FMR linewidths are generally dominated by inhomogeneous broadening and the typical value in these films is in the order of 50 Oe at 20 K. In contrast, the linewidths of (Ga,Mn)As film previously reported for x = 0.05 are in 100–300 Oe range. Our results show an inhomogeneous linewidth being exceptionally low, demonstrating that these layers are of exceptional magnetic homogeneity, with no gradient in the Mn concentrations and no Mn clustering effects [57].

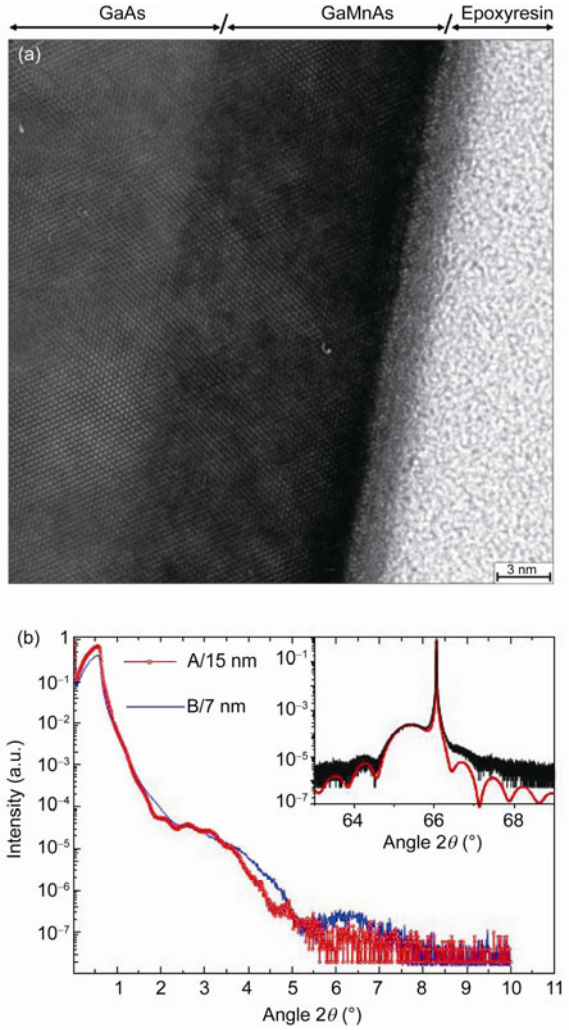

Figure 4 (a) High-resolution cross-sectional transmission electron microscopy image of a 15 nm $Ga_{1-x}Mn_xAs$ film; (b) high-resolution X-ray reflection spectra of both 15 nm and 7 nm $Ga_{1-x}Mn_xAs$ films. The inset of (b) is a HRXRD spectrum (black line) and its simulation (red dotted line) for 15 nm $Ga_{1-x}Mn_xAs$ film. Here x_{nomi} = 25% [57].

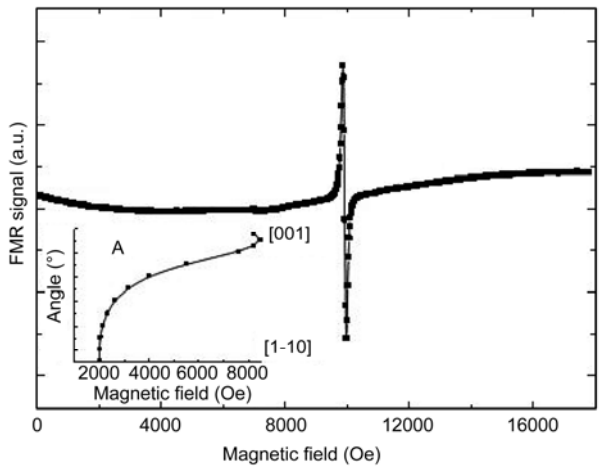

Figure 5 Large scale FMR spectrum at T = 60 K for H//[001] of the 15 nm $Ga_{1-x}Mn_xAs$ film with x = 25%, as shown in Figure 4. Inset: angular variation in the FMR resonance field for an out-of-plane variation (squares), and a theoretical fit (line) [57].

On the other hand, magnetic circular dichroism (MCD) and anomalous Hall effect (AHE) are usually used to judge whether the ferromagnetism is intrinsic or not. The hysteresis behavior of the MCD (Figure 6) and AHE signal (Figure 7) also demonstrate the intrinsic ferromagnetism of the heavy Mn doping (Ga,Mn)As sample [58].

When grown at the substrate temperature T_{sub} about 250°C, GaAs films usually contain double donor As_{Ga} defects at concentration As_{Ga} ~10^{20} cm^{-3}, that is about 1% of Ga sites [59,60]. For a fixed V/III BEP ratio, As_{Ga} in low-temperature GaAs increases exponentially as T_{sub} decreases below 300°C [61,62]. Based on this idea, our group obtained T_C ~ 141 K in as-grown heavily Mn-doped (Ga,Mn)As films with the thickness of 10 nm by setting V/III BEP ratio at 8. The x_{nomi} is 20%, and the *in-situ* reflection high energy electron diffraction (RHEED) patterns still remained streaky (1×2) as that observed in the conventional (Ga,Mn)As during growth, showing two-dimensional growth mode. After being annealed in air at 140°C for 16 h, T_C increases to 191 K [27]. Figure 8 shows the temperature dependence of the remnant magnetization of the 10 nm (Ga,Mn)As film, and the inset is the magnetization hysteresis loops measured at 5, 170 and 190 K, respectively, verifying the ferromagnetic state persists up to 190 K.

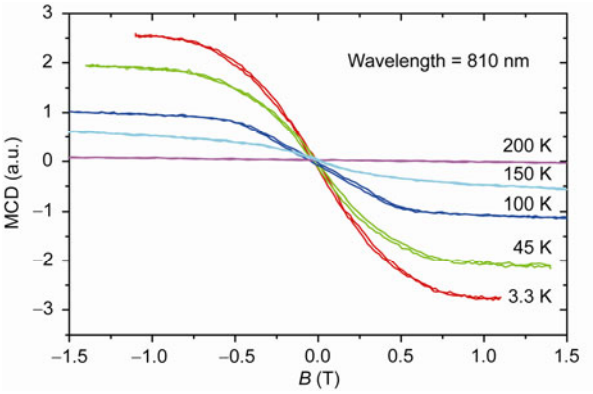

Figure 6 MCD signals of a typical heavy Mn doping (Ga,Mn)As film measured at different temperatures [58].

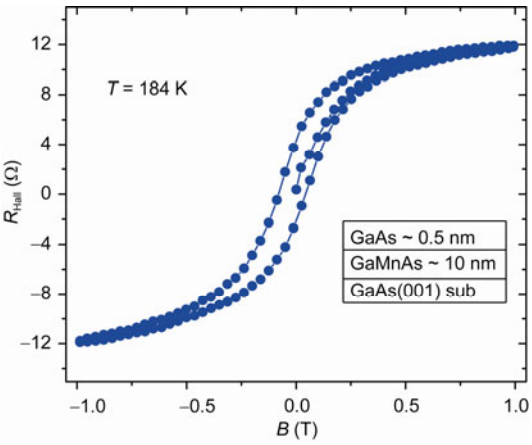

Figure 7 Magnetic field dependence of the anomalous Hall resistance R_{Hall} of a typical heavy Mn doping (Ga,Mn)As film [58].

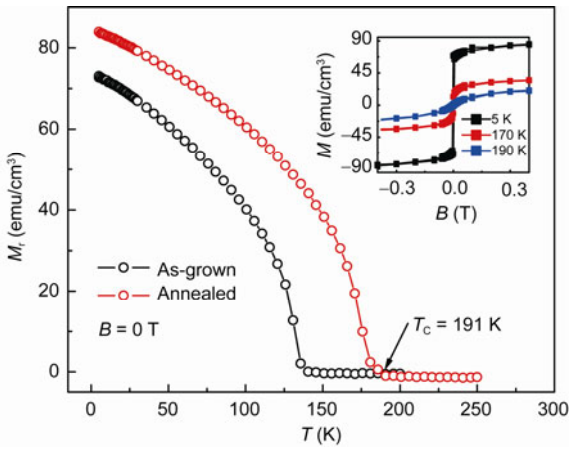

Figure 8 Temperature dependence of the remnant magnetization of a 10 nm heavily Mn-doped (Ga,Mn)As film measured by SQUID magnetometer. The inset shows the magnetization hysteresis loops measured at 5, 170 and 190 K with the magnetic field along the [–110] direction [27].

4 Nanostructure engineering

Experimental data show that the effective Mn content is lower than the nominal one in the heavy Mn doping case, which indicates that a large fraction of Mn ions goes into the interstitial sites [3,63]. It has been shown by Samarth's group [26,64] that T_C of a GaAs-capped (Ga,Mn)As layer with moderate Mn-doping (~6%) can be enhanced via a combination of nanopatterning and annealing. In their work, accompanying by a significant decrease in the resistivity of the patterned wire, was an increase in T_C of almost 50 K. It was postulated that nanostructures facilitate the diffusion of Mn interstitials toward sidewalls, thus enhancing the effect of annealing. This scheme is expected to be even more effective in samples with heavy Mn doping because of the larger density of Mn interstials.

Inspired by these ideas, we tried to apply the nanofabrication method to our heavy doping samples. The growth details of the samples were described in the previous section. The nominal Mn concentration x_{nomi} of the film was estimated by HRXRD. According to Vegard's law, the lattice constant $a = (0.566(1–x) + 0.598x)$ nm. Here, $a = 0.566$ nm for $x = 0$ is the lattice constant of GaAs grown at low temperature, and $a = 0.598$ nm for $x = 1$ is the lattice constant of hypothetical zincblende MnAs. Because the (Ga,Mn)As layer is fully strained on GaAs, the free-standing lattice constant of (Ga,Mn)As can be calculated from the formula $a = [(1–\nu)/(1+\nu)]a_{XRD} + [(2\nu)/(1+\nu)]a_{GaAs}$ [65], where a_{XRD} is the measured lattice constant, a_{GaAs} is the lattice constant of GaAs, and ν is the Poisson ratio. Figure 9 shows the ω-2θ scan of the film used for patterning near the GaAs (004)

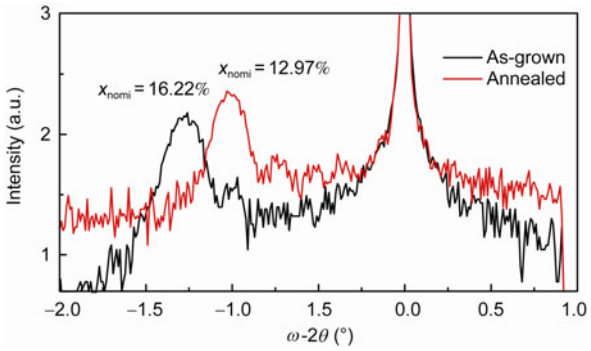

Figure 9 ω-2θ scan of the heavy Mn doping (Ga,Mn)As film near the GaAs (004) substrate peak before and after annealing [28].

peak of the substrate. The x_{nomi} is estimated to be 16.2% for the as-grown state and decreases to 13.0% after annealing in air at 160°C for 13 h. In order to establish the evolution of the magnetic properties of the film with annealing, eight pieces were cut from the same wafer and annealed at 160°C for various durations of time. Magnetic measurements were performed on each sample with a commercial superconducting quantum interference device (SQUID) magnetometer. Figure 10 shows a set of temperature dependent remnant magnetization M_r for the film in the as-grown state and at various annealing times. We can see that T_C reaches a maximum after annealing for 2 h and remains at this value even after annealing for 46 h, which shows the absence of any detrimental effect from over annealing in this sample at this annealing temperature. Magnetic hysteresis measurements show a hard magnetic axis perpendicular to the plane because of compressive strain; the in-plane magnetic easy axis is along the [−110] direction. The low-temperature annealing process reduces the Mn interstitial density and improves the quality of the (Ga,Mn)As, that is, increasing its hole density, magnetic moment, and T_C [23,36]. The effective Mn concentration of the annealed sample was 8.6% based on the saturation magnetization M_S measured at 5 K and the assumption of S = 5/2 for each substitutional Mn_{Ga} atom. This is smaller than x_{nomi} = 13.0% determined by HRXRD and indicates that the Mn interstitials have not been entirely removed.

The nanowire devices used for the magnetotransport measurements were fabricated in two steps. First, a standard Hall bar with width and length of 5 and 10 μm, respectively, was produced by optical lithography and wet etching by a solution of $H_3PO_4/H_2O_2/H_2O$ = 1:1:38. Then a nanowire structure with desired width was defined on top of the active channel of the large Hall bar by EBL, using 200 nm thick poly-methylmethacrylate (PMMA) resist and a MIBK/IPA = 3:1 developer. The pattern was transferred from PMMA to the (Ga,Mn)As layer by wet etching in the same etching solution. All the devices were patterned so that the lengths of the nanowires are oriented along the [110] direction. During the patterning process, all samples were subject to the same thermal treatments, and the highest baking temperature was 110°C. Figures 11(a)–(d) shows four typical scanning electron microscopy (SEM) images of the nanowires devices with channel widths from 156 to 686 nm.

Because the magnetic moment of each nanowire is minute compared to that of the larger continuous films and too small to be detected by the SQUID magnetometer, we determined T_C by using transport measurements carried out in a physical property measurement system (PPMS). The magnetotransport measurements were performed with the magnetic field B perpendicular to the sample plane. The Hall resistance R_{Hall} and longitudinal resistance R were measured by standard four-probe method. To avoid any Joule heating, a bias current I = 50 nA was used in all the measurements.

Since the temperature dependence of the resistance, particularly the well-defined peak of the metal to insulator transition near the ferromagnetic transition, has been widely used to determine T_C in (Ga,Mn)As [26,36,64]. We first

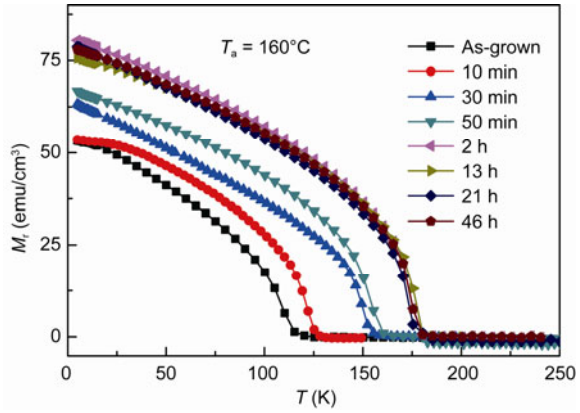

Figure 10 Temperature dependent remnant magnetization of 8 pieces of unpatterned (Ga,Mn)As films subjected to different annealing duration at 160°C. All of them were cut from the same sample used for patterning [28].

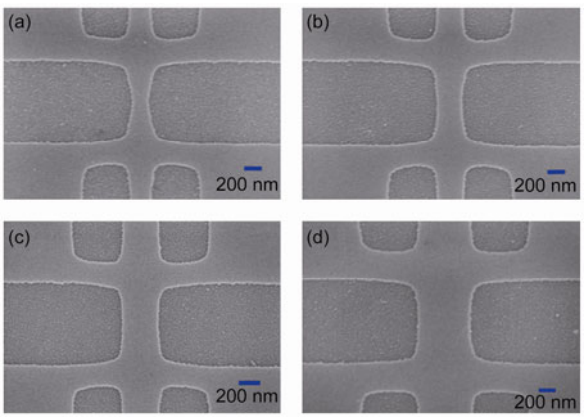

Figure 11 SEM images of the nanowire devices with widths of (a) 156 nm, (b) 255 nm, (c) 310 nm, and (d) 686 nm. All the lengths of the hall bar are oriented along the [110] direction [28].

probed T_C by measuring the resistance as a function of temperature. The positions of the resistance peaks were determined from the derivatives of $R(T)$ by calculating the temperature at which $dR/dT = 0$. On the basis of the theory of Fisher and Langer [66], the position of T_C on the $R(T)$ curve is dependent on the magnitude of the wave vector of the carriers (carrier density). In the case of (Ga,Mn)As, whose carrier density lies in between the extremes for insulating concentrated magnetic semiconductors and ferromagnetic metals, the location of T_C on the $R(T)$ curve has been found to be sample dependent. In some samples T_C is located at the resistance peak ($dR/dT = 0$) [26,36,64] while in others at the maximum for dR/dT [46]. Therefore, for a particular set of samples, it is crucial to establish experimentally the proper criterion for T_C determination from $R(T)$. We have done so for our heavily Mn-doped continuous film, via direct comparison of the temperature dependent magnetization and resistance measurements on the same sample. The results are shown in Figure 12. It is clear that the T_C determined from $M_r(T)$ coincides with the peak in $R(T)$ ($dR/dT = 0$), which provided the basis for using $dR/dT = 0$ as the criterion for determining T_C in our samples. For the nanowires, we further provided a rigorous and independent confirmation of the value of T_C by Arrott plots derived from AHE. Finally, we demonstrated in Figure 13 that the temperature dependencies of the resistivity are identical when measured

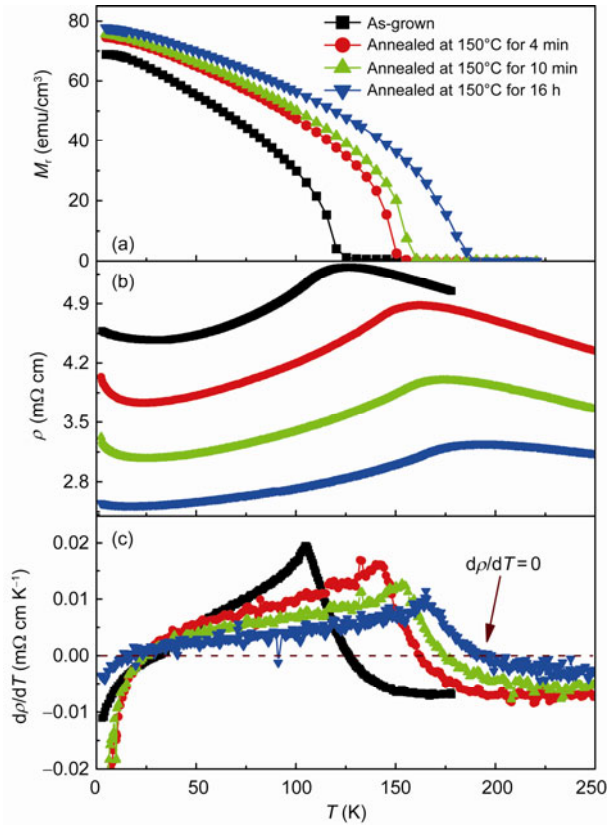

Figure 12 Temperature dependence of (a) remnant magnetization, (b) resistivity, and (c) temperature derivative of resistivity of (Ga,Mn)As [28].

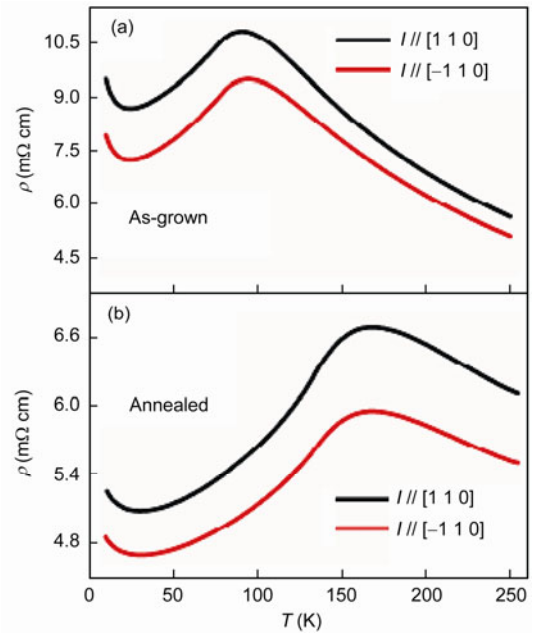

Figure 13 Temperature dependence of the resistivity of two 5-μm devices in (a) as-grown, and (b) annealed states. The lengths of the two devices are oriented along two different crystalline directions [28].

along different crystalline orientations despite the strong in-plane magnetic anisotropy in the heavily Mn-doped (Ga,Mn)As film.

Figure 14 shows the temperature dependence of the resistance of a nanowire device with 310 nm width. It shows metallic behavior which is similar to a conventional metallic (Ga,Mn)As film. Below about 35 K, the resistance shows an upturn, probably because of the electron-electron interactions [67]. T_C of the as-made device, as determined by the resistance peak of the R-T curve, increases to (167 ± 5) K, up from 125 K for the as-grown film (shown in Figure 10). This is most likely because of unintentional annealing during the sample processing.

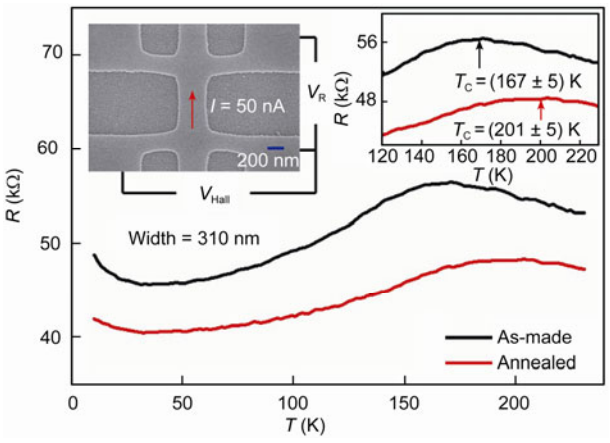

Figure 14 Temperature dependence of the resistance of a device with w = 310 nm in the as-made (black) state and after annealing (red). Left inset shows the experimental geometry. Right inset shows the close-up view around T_C. All the measurements were done with a current I = 50 nA [28].

Figure 15(a) shows the temperature dependent resistance curves of a number of as-made devices with different widths, and T_C for each device is summarized in Figure 15(c). We can see that the resistance increases monotonically as the width decreases, and T_C is nearly the same for different widths (from 156 nm to 5 μm). No obvious quantum confinement effect was observed in this size range. Figure 15(b) shows the temperature dependence of the resistance of the same devices after annealing in air at 160°C for 13 h. T_C values for the annealed samples, as determined from the resistance maximum of the *R-T* curves, are also summarized in Figure 15(c). T_C is increased to more than 190 K for the devices from 255 to 686 nm. This is in comparison to the device with 5 μm width, which has a T_C of about 180 K, similar to the T_C determined from the SQUID magnetization measurement for the unpatterned film (Figure 10). The T_C enhancement reaches a maximum at wire width to approximately 310 nm, where T_C is increased to as high as (201 ± 5) K as evidenced by *R-T* measurements (also shown in Figure 14). At even smaller wire widths, T_C decreases from this highest value.

To eliminate the possibility that the variation of T_C with wire width is an artifact caused by under or over annealing of the wires, two series of nanowire devices with widths of 233 and 310 nm were fabricated and each device annealed at 160°C for various durations. As shown in Figures 16(a) and (b), for both groups of devices, 13 h of annealing was sufficient to reach saturation and additional annealing did not cause any T_C degradation. This is qualitatively consistent with the trend shown in Figure 10 for the unpatterned films and demonstrates that all the devices were optimally annealed.

We attribute the observed T_C enhancement in the nanowires to the increase of the free surface, which allows the Mn interstitials to diffuse out at the sidewalls, thus enhancing the efficiency of annealing. Considering the geometry of the devices, length l, width w, and height h, the increased free surface at sidewalls is $2lh$. The percentage increase in the free surface is $2lh/lw = 6\%$ for $h = 10$ nm and $w = 310$ nm, while for the device with 5 μm width the free surface only increases by 0.4%. We show here that the free surface increase of 6% at sidewalls is critical for the annealing of (Ga,Mn)As, which results in an 11% T_C increase (from 180 to 200 K). We conclude that the nanostructure patterning greatly enhances the effect of thermal annealing. For the narrowest devices with widths of 156 and 188 nm, which have even larger free surface increases, the increase of T_C after annealing is less than those of the devices with more moderate widths (255 and 310 nm). We surmise that this is because of strain relaxation induced by the lithographic patterning and annealing when the width becomes less than 200 nm, which could degrade the crystalline quality of (Ga,Mn)As [68]. To confirm that strain relaxation was responsible for the T_C reduction in the narrowest wires, we fabricated and measured a series of nanowires patterned from another piece of film that had been optimally annealed at 160°C for 13 h. The nanowires underwent no additional annealing after patterning and care was taken to avoid any unintentional annealing during the patterning process (the baking temperature never exceeded 110°C). The results are shown in Figure 17. No T_C enhancement is seen with decreasing wire width, and a small reduction of T_C (about 5–7 K) is observed when the width becomes smaller than 500 nm. These results convincingly demonstrate that strain

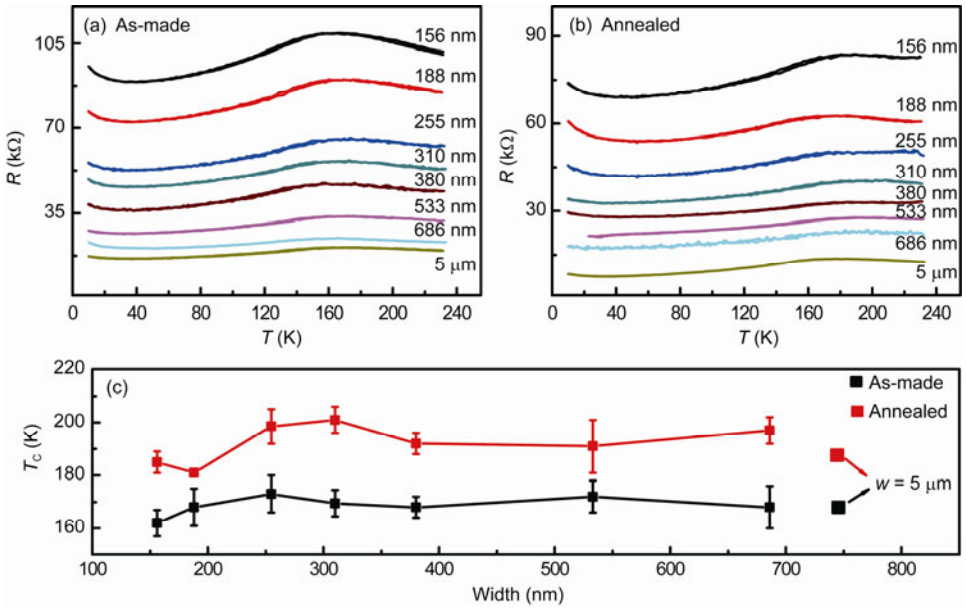

Figure 15 Temperature dependence of the resistance of several devices with different widths in (a) as-made and (b) annealed states. T_C values determined from the resistance maximum of *R-T* curves are summarized in (c) [28].

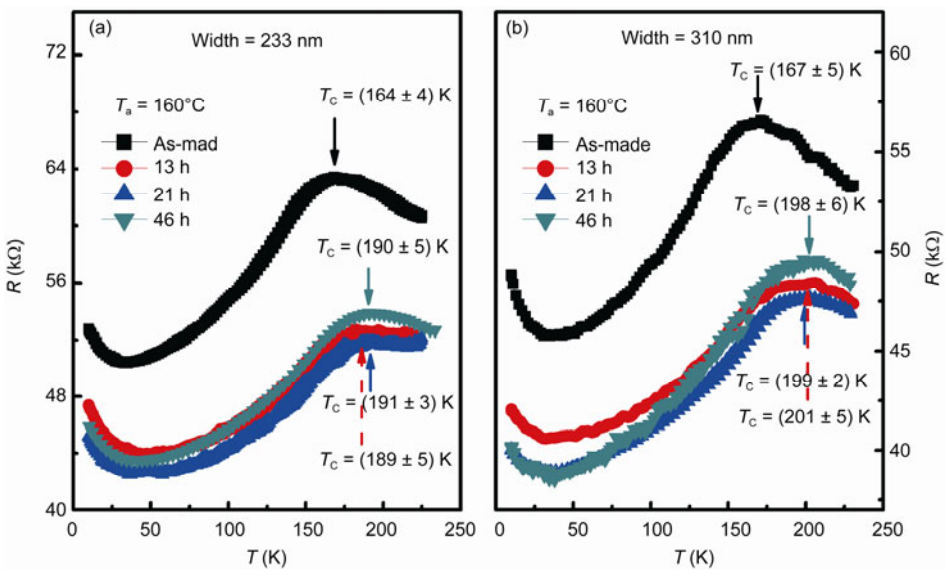

Figure 16 Temperature dependent resistance curves of two series of nanowires with widths of (a) 233 nm and (b) 310 nm in the as-made state and after different annealing times as indicated [28].

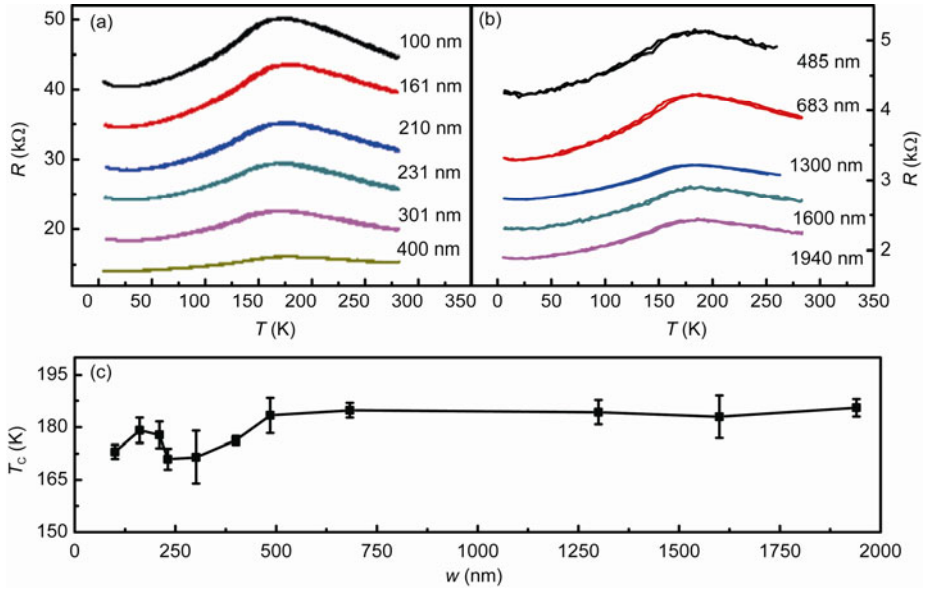

Figure 17 Temperature dependence of the resistance of nano-structure devices with widths ranging from (a) 100 nm to 400 nm and (b) from 485 nm to 1940 nm. T_C values determined from the resistance maximum of *R-T* curves are summarized in (c) [28].

relaxation induced by the lithographic patterning would decrease T_C. Furthermore, several other nanowire devices based on (Ga,Mn)As films of different thickness and Mn concentration have been fabricated. The nanowires from a thicker (18 nm) (Ga,Mn)As film with similar heavy Mn doping (x_{nomi} = 14.3%) exhibit maximum T_C enhancement quantitatively consistent with the results presented above. In contrast, for the moderately Mn-doped (Ga,Mn)As film (x_{nomi} = 7.5%), the magnitude of T_C enhancement is significantly smaller than that in either of the heavily Mn-doped (Ga,Mn)As samples.

In discussing Figure 14, we alluded to the fact that determining T_C from the *R-T* curve is not ideal with an error bar of several K. Here, we used Arrott plots to accurately determine T_C beyond any ambiguity. The magnetic field dependence of the Hall resistance R_{Hall} and resistance R measured at different temperature is shown in Figures 18(a) and (b). The Hall resistance of (Ga,Mn)As can be written as $R_{Hall} = R_0B/d + R_SM/d$, where R_0 is the ordinary Hall coefficient, R_S is the anomalous Hall coefficient, d is the sample thickness, B and M are the magnetic induction and magnetization perpendicular to the sample surface, respectively [3]. The anomalous Hall component is the dominant one at low field, and a scaling relation $R_S/d = cR^2$ (c is a constant) is

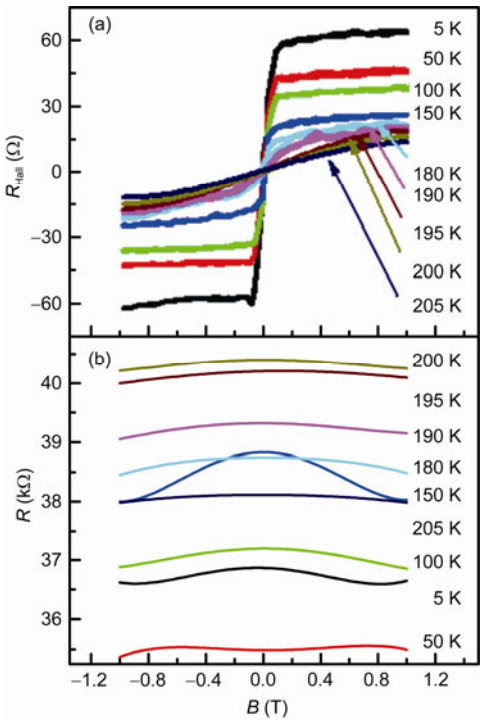

Figure 18 Magnetic field dependence of the (a) Hall resistance and (b) resistance of the annealed device with w = 310 nm measured at different temperatures [28].

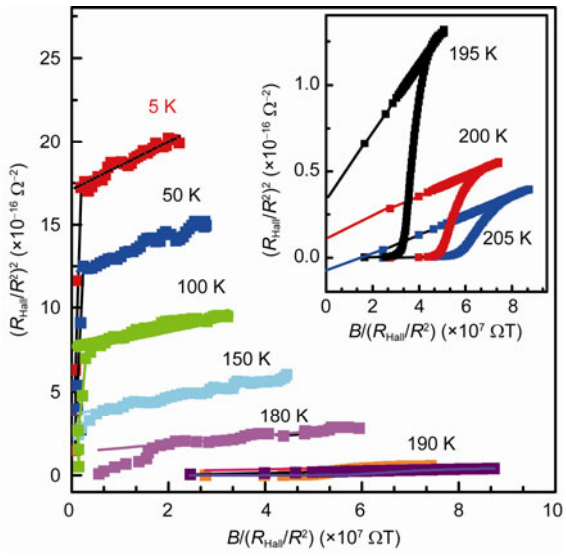

Figure 19 Arrott plots at different temperature. The inset shows a close-up view of the Arrott plots near the ferromagnetic transition, which confirms T_C is slightly above 200 K [28].

expected because of the dominance of the Berry-phase mechanism in the metallic regime [69–71]. Thus, the ratio of R_{Hall}/R^2 can be used to track the magnetization. In the Arrott plots, $(R_{Hall}/R^2)^2$ versus $B/(R_{Hall}/R^2)$, a ferromagnetic state corresponds to a positive extrapolated ordinate intercept, while paramagnetic state corresponds to a negative extrapolated intercept [72]. In Figure 19, the extrapolated intercept remains positive at 200 K and turns negative at 205 K, indicating that T_C is between those extrema and somewhat higher than 200 K. We point out that due to the very small magnetoresistance in the relevant temperature range (Figure 18(b)) and the use of a different scaling relation has negligible effect on the outcome of the Arrott plots analysis.

5 Conclusions

Despite extensively research in the past fifteen years, there are still many debates about (Ga,Mn)As such as the band picture and whether T_C can be raised up to room temperature. Here, combining the theoretical and experimental results, conclusions and prospects are made as follows.

Firstly, in the case of moderate Mn doping (<10%), T_C increases linearly with the concentration x_{eff} of local Mn_{Ga} moments participating in the ordered ferromagnetic state [35]. Secondly, utilizing the LT-MBE technique, high-quality heavily Mn-doped (>10%) (Ga,Mn)As films can be obtained by careful tuning of the growth parameters [27,44, 53–56]. Thirdly, post-growth annealing at appropriate temperature in air or O_2 can move out the Mn interstitials, which compensate the holes and couple with the adjacent Mn_{Ga} antiferromagnetically, thus can enhance T_C efficiently [21–26]. Annealing efficiency can be improved by increasing the free surface of (Ga,Mn)As via micro- or nano-fabrication which can raise T_C further more in (Ga,Mn)As nano-stuctures [26,28]. Fourthly, although the highest T_C of (Ga,Mn)As single layer is 200 K, there is still a space to further enhance this by optimizing growth parameters, nano-fabrication technique and post-growth annealing conditions. Lastly, ferromagnetic proximity effect existing in ferromagnet/(Ga,Mn)As bilayers seems to be a promising method to increase T_C of (Ga,Mn)As to room temperature [48].

The authors acknowledge DENG JiaJun, ZHU Ke, ZHENG HouZhi, MISURACA Jennifer, XIONG Peng, von MOLNÁR Stephan, KHAZEN, Kh. and von BARDELEBEN H. J. for their collaborations. This work was supported by the National Natural Science Foundation of China (Grant Nos. 60836002, 11127406 and 10920101071).

1 Jungwirth T, Sinova J, Masek J, et al. Theory of ferromagnetic (III,Mn)V semiconductors. Rev Mod Phys, 2006, 78: 809–864
2 Wolf S A, Awschalom D D, Buhrman R A, et al. Spintronics: A spin-based electronics vision for the future. Science, 2001, 294: 1488–1495
3 Ohno H. Making nonmagnetic semiconductors ferromagnetic. Science, 1998, 281: 951–956
4 Zhao J H, Deng J J, Zheng H Z. Diluted magnetic semiconductors (in Chinese). Prog Phys, 2007, 27: 109–150
5 Von Molnar S, Reed D. New materials for semiconductor spin-electronics. Proc IEEE, 2003, 91: 715–726
6 Furdyna J K. Diluted magnetic semiconductors. J Appl Phys, 1988, 64: R29–R64

7 Ohno H, Munekata H, Penney T, et al. Magnetotransport properties of p-type (In,Mn) As diluted magnetic III-V semiconductors. Phys Rev Lett, 1992, 68: 2664–2667
8 Munekata H, Ohno H, Von Molnar S, et al. Diluted magnetic III-V semiconductors. Phys Rev Lett, 1989, 63: 1849–1852
9 Ohno H, Shen A, Matsukura F, et al. (Ga,Mn)As: A new diluted magnetic semiconductor based on GaAs. Appl Phys Lett, 1996, 69: 363–365
10 Kreissl, J, Ulrici W, El-Metoui M, et al. Neutral manganese acceptor in GaP: An electron-paramagnetic-resonance study. Phys Rev B, 1996, 54: 10508–10515
11 Kronik L, Jain M, Chelikowsky J R. Electronic structure and spin polarization of MnGaN. Phys Rev B, 2002, 66: 041203
12 Dietl T, Ohno H, Matsukura F, et al. Zener model description of ferromagnetism in Zinc-Blende magnetic semiconductors. Science, 2000, 287: 1019–1022
13 Ohno H, Chiba D, Matsukura F, et al. Electric-field control of ferromagnetism. Nature, 2000, 408: 944–946
14 Ohno Y, Young D K, Beschoten B, et al. Electrical spin injection in a ferromagnetic semiconductor heterostructure. Nature, 1999, 402: 790–792.
15 Gould C, Ruster C, Jungwirth T, et al. Tunnelling anisotropic magnetoresistance: A spin-valve like tunnel magnetoresistance using a single magnetic layer. Phys Rev Lett, 2004, 93: 117203
16 Chiba D, Yamanouchi M, Matsukura F, et al. Electrical manipulation of magnetization reversal in a ferromagnetic semiconductor. Science, 2003, 301: 943–945
17 Chiba D, Sawicki M, Nishitani Y, et al. Magnetization vector manipulation by electric fields. Nature, 2008, 455: 515–518
18 Chernyshov A, Overby M, Liu X Y, et al. Evidence for reversible control of magnetization in a ferromagnetic material by means of spin–orbit magnetic field. Nat Phys, 2009, 5: 656–659
19 Sawicki M, Chiba D, Korbecka A, et al. Experimental probing of the interplay between ferromagnetismand localization in (Ga,Mn)As. Nat Phys, 2009, 6: 22–25
20 Yamanouchi M, Chiba D, Matsukura F, et al. Current-induced domain-wall switching in a ferromagnetic semiconductor structure. Nature, 2004, 428: 539–541
21 Hayashi T, Hashimoto Y, Katsumoto S, et al. Effect of low-temperature annealing on transport and magnetism of diluted magnetic semiconductor (Ga,Mn)As. Appl Phys Lett, 2001, 78: 1691–1693
22 Edmonds K W, Wang K Y, Campion R P, et al. High Curie temperature GaMnAs obtained by resistance-monitored annealing. Appl Phys Lett, 2002, 81: 4991–4993
23 Yu K M, Walukiewicz W. Effect of the location of Mn sites in ferromagnetic GaMnAs on its Curie temperature. Phys Rev B, 2002, 65: 201303R
24 Chiba D, Takamura K, Matsukura F, et al. Effect of low-temperature annealing on (Ga,Mn)As trilayer structures. Appl Phys Lett, 2003, 82: 3020–3022
25 Ku K C, Potashnik S J, Wang R F, et al. Highly enhanced Curie temperature in low-temperature annealed GaMnAs epilayers. Appl Phys Lett, 2003, 82: 2302–2304
26 Eid K F, Sheu B L, Maksimov O, et al. Nanoengineered Curie temperature in laterally patterned ferromagnetic semiconductor heterostructures. Appl Phys Lett, 2005, 86: 152505
27 Chen L, Yan S, Xu P F, et al. Low-temperature magnetotransport behaviors of heavily Mn-doped (Ga,Mn)As films with high ferromagnetic transition temperature. Appl Phys Lett, 2009, 95: 182505
28 Chen L, Yang X, Yang F H, et al. Enhancing the Curie temperature of ferromagnetic semiconductor (Ga,Mn)As to 200 K via nanostructure engineering. Nano Lett, 2011, 11: 2584–2589
29 Dobrowolska M, Tivakornsasithorn K, Liu X Y, et al. Controlling the Curie temperature in (Ga,Mn)As through location of the Fermi level within the impurity band. Nat Mater, 2012, 11: 444–449
30 Ohya S, Takata K, Tanaka M, et al. Nearly non-magnetic valence band of the ferromagnetic semiconductor GaMnAs. Nat Phys, 2011, 7: 342–347
31 Wang W Z, Deng J J, Lu J, et al. Influence of Si doping on magnetic properties of (Ga,Mn)As. Phys E, 2008, 41: 84–87
32 Cho Y J, Yu K M, Liu X Y, et al. Effects of donor doping on GaMnAs. Appl Phys Lett, 2008, 93: 262505
33 Schott G M, Ruster C, Brunner K, et al. Doping of low-temperature GaAs and GaMnAs with carbon. Appl Phys Lett, 2004, 85: 4678–4680
34 Dietl T, Ohno H, Matsukura F, et al. Hole-mediated ferromagnetism in tetrahedrally coordinated semiconductors. Phys Rev B, 2001, 63: 192505
35 Jungwirth T, Wang K Y, Masek J, et al. Prospects for high temperature ferromagnetism in (Ga,Mn)As semiconductors. Phys Rev B, 2005, 72: 165204
36 MacDonal A H, Schiffer P, Samarth N. Ferromagnetic semiconductors: moving beyond (Ga,Mn)As. Nat Mater, 2005, 4: 195–202
37 Onomitsu K, Fukui H, Maeda T, et al. Mn and Be codoped GaAs for high hole concentration by low-temperature migration-enhanced epitaxy. J Vac Sci Technol B, 2004, 22: 1746–1749
38 Yu K M, Walukiewicz W, Wojtowicz T, et al. Curie temperature limit in ferromagnetic GaMnAs. Phys Rev B, 2003, 68: 041308R
39 Park Y D, Lim J D, Suh K S, et al. Carrier-mediated ferromagnetic ordering in Mn ion-implanted p^+ GaAs:C. Phys Rev B, 2003, 68: 085210
40 Ibanez J, Edmonds K W, Henini M, et al. Electrical characterisation of (Ga,Mn,Cr)As thin films grown by molecular beam epitaxy. J Cryst Growth, 2005, 278: 695–698
41 Wang K Y, Edmonds KW, Zhao L X, et al. (Ga,Mn)As grown on (311) GaAs substrates: Modified Mn incorporation and magnetic anisotropies. Phys Rev B, 2005, 72: 115207
42 Wurstbauer U, Sperl M, Soda M, et al. Ferromagnetic GaMnAs grown on (110) faced GaAs. Appl Phys Lett, 2008, 92: 102506
43 Wang K Y, Campion R P, Edmonds K W, et al. Magnetism in (Ga,Mn)As thin films with T_C up to 173 K. AIP Conf Proc, 2005, 772: 333–334
44 Ohno K, Ohya S, Tanaka M. Properties of heavily Mn-doped GaMnAs with Curie temperature of 172.5 K. J Supercond Nov Magn, 2007, 20: 417–420
45 Bliss D E, Walukiewicz W, Ager J W, et al. Annealing studies of lowtemperaturegrown GaAs:Be. J Appl Phys, 1992, 71: 1699–1707
46 Novak V, Olejnik K, Wunderlich J, et al. Curie point singularity in the temperature derivative of resistivity in (Ga,Mn)As. Phys Rev Lett, 2008, 101: 077201
47 Xu J L, Van Schilfgaarde M. Role of disorder in Mn:GaAs, Cr:GaAs, and Cr:GaN. Phys Rev Lett, 2005, 94: 097201
48 Raebiger H, Ayuela A, Von Boehm J. Electronic and magnetic properties of substitutional Mn clusters in (Ga,Mn)As. Phys Rev B, 2005, 72: 014465
49 Raebiger H, Ganchenkova M, Von Boehm J. Diffusion and clustering of substitutional Mn in GaMnAs. Appl Phys Lett, 2006, 89: 012505
50 Hynninen T, Gnachenkova M, Raebiger H, et al. Ferromagnetism and its evolution during long-term annealing in (Ga,Mn)As. Phys Rev B, 2006, 74: 195337
51 Nazmul A M, Amemiya T, Shuto Y, et al. High temperature ferromagnetism in GaAs-based heterostructures with Mn δ doping. Phys Rev Lett, 2005, 95: 017201
52 Song C, Sperl M, Utz M, et al. Proximity induced enhancement of the Curie temperature in hybrid spin injection devices. Phys Rev Lett, 2011, 107: 056601
53 Chiba D, Nishitani Y, Matsukura F, et al. Properties of $Ga_{1-x}Mn_xAs$ with high Mn composition (x>0.1). Appl Phys Lett, 2007, 90: 122503
54 Chiba D, Yu K M, Walukiewicz W, et al. Properties of $Ga_{1-x}Mn_xAs$ with high x (> 0.1). J Appl Phys, 2008, 103: 07D136
55 Mack S, Myers R C, Heron J T, et al. Stoichiometric growth of high Curie temperature heavily alloyed GaMnAs. Appl Phys Lett, 2008, 92: 192502
56 Ohya S, Ohno K, Tanaka M. Magneto-optical and magnetotransport properties of heavily Mn-doped GaMnAs. Appl Phys Lett, 2007, 90: 112503
57 Khazen Kh, Von Bardeleben H J, Cantin J L, et al. Intrinsically lim-

ited critical temperatures of highly doped $Ga_{1-x}Mn_xAs$ thin films. Phys Rev B, 2010, 81: 235201
58 Zhu K. Study on Magneto-optical Properties of Diluted Magnetic Semiconductors. Dissertation for Doctoral Degree. Beijing: Institute of Semiconductors, Chinese Academy of Sciences, 2010
59 Liu X, Prasad A, Nishio J, et al. Native point defects in low temperature grown GaAs. Appl Phys Lett, 1995, 67: 279–281
60 Missous M, O'Hagan S. Nonstoichiometry and dopants related phenomena in low temperature GaAs grown by molecular beam epitaxy. J Appl Phys, 1993, 75: 3396–3401
61 Luysberg M, Sohn H, Prasad A, et al. Effects of the growth temperature and As/Ga flux ratio on the incorporation of excess As into low temperature grown GaAs. J Appl Phys, 1997, 83: 561–566
62 Suda A, Otsuka N. Surface atomic process of incorporation of excess arsenic in molecular-beam epitaxy of GaAs. Surf Sci, 2000, 458: 162–172
63 Dietl T. A ten-year perspective on dilute magnetic semiconductors and oxides. Nat Mater, 2010, 2898: 965–974
64 Sheu B L, Eid K F, Maksimov O, et al. Width dependence of annealing effects in (Ga,Mn)As nanowires. J Appl Phys, 2006, 99: 08D501
65 Awschalom D D, Loss D, Sarmarth N, et al. Semiconductor Spintronics and Quantum Computation. Berlin: Springer, 2002
66 Fisher M E, Langer J S. Resistive anomalies at magnetic critical points. Phys Rev Lett, 1968, 20: 665–668
67 Neumaier D, Schlapps M, Wurstbauer U, et al. Electron-electron interaction in one- and two-dimensional ferromagnetic GaMnAs. Phys Rev B, 2008, 77: 041306
68 Wenisch J, Gould C, Ebel L, et al. Control of magnetic anisotropy in (Ga,Mn)As by lithography-induced strain relaxation. Phys Rev Lett, 2007, 99: 077201
69 Jungwirth T, Niu Q, MacDonald A H. Anomalous Hall effect in ferromagnetic semiconductors. Phys Rev Lett, 2002, 88: 207208
70 Chun S H, Kim Y S, Choi H K, et al. Interplay between carrier and impurity concentrations in annealed $Ga_{1-x}Mn_xAs$: Intrinsic anomalous Hall effect. Phys Rev Lett, 2007, 98: 026601
71 Pu Y, Chiba D, Matsukura F, et al. Mott relation for anomalous Hall and Nernst effects in$Ga_{1-x}Mn_xAs$ ferromagnetic semiconductors. Phys Rev Lett, 2008, 101: 117208
72 Arrott A. Criterion for ferromagnetism from observations of magnetic isotherias. Phys Rev, 1957, 108: 1394–1396